J Solid State Electrochem (2015) 19:2075–2085
DOI 10.1007/s10008-014-2726-2

ORIGINAL PAPER

Preparation of ordered and oriented mesoporous silica thin films bearing octyl or hexadecyl groups by electrochemically assisted self-assembly and evaluation of their transport properties

Christelle Despas · Nataliya A. Vodolazkaya · Jaafar Ghanbaja · Alain Walcarius

Received: 14 November 2014 / Accepted: 25 December 2014 / Published online: 18 January 2015

Abstract Well-organized octyl- and hexadecyl-functionalized mesoporous silica thin films are generated onto indium-tin oxide electrodes by combining the electrochemically assisted self-assembly technique and the sol–gel co-condensation route. The electrodeposition is carried out under potential control from mixtures containing various molar ratios of tetraethoxysilane and octyltrimethoxysilane (O-TES) or hexadecyltrimethoxysilane (HD-TES), using cetyltrimethylammonium bromide as surfactant template. Films with hexagonally packed functionalized mesochannels oriented perpendicular to the underlying support are obtained up to, respectively, 20 % O-TES and 5 % HD-TES introduced in the starting sol. Electrochemical investigations using various redox probes demonstrate that the films remain porous despite the presence of long carbon chains inside the mesochannels and that, in the presence of such long chain alkyl groups, the physical diffusion through the pores is not sufficient to describe the mass transport issues, which can also imply accumulation effects owing to the hydrophobic character of the medium.

Keywords EASA (electro-assisted self-assembly) · Mesoporous silica film · Octylsilane · Hexadecylsilane · Hydrophobic/hydrophilic balance

C. Despas (✉) · N. A. Vodolazkaya · A. Walcarius
Laboratoire de Chimie Physique et Microbiologie pour l'Environnement, UMR 7564, CNRS-Université de Lorraine, 405, rue de Vandoeuvre, 54600 Villers-les-Nancy, France
e-mail: christelle.despas@univ-lorraine.fr

N. A. Vodolazkaya
Chemical Faculty, Department of Physical Chemistry, V.N. Karazin Kharkov National University, 61077 Kharkov, Ukraine

J. Ghanbaja
Institut Jean Lamour, UMR 7198, CNRS-Université de Lorraine, Villers-les-Nancy, France

Introduction

Electrogeneration of porous layers on electrode surfaces via bottom-up approaches using molecular templates, supramolecular assemblies, or suitable spatial arrangements of macromolecules or micro- and nano-objects has become a field of growing interest [1–3]. The main motivations beyond these template approaches rely on advantages belonging to such highly porous film electrodes in terms of improved performance in sensitivity due to much higher electroactive surface areas and accelerated mass transport issues in comparison to conventional electrodes, and also on getting nano-engineered electrode surfaces with unprecedented hosting properties for reactants (biomolecules, catalysts, etc.). A variety of functional materials with diverse structures and morphologies such as one-dimensional nanostructures, two-dimensional films, and three-dimensional porous frameworks have been synthesized with the aid of "hard" or "soft" templates. Track-etched polycarbonate, anodized alumina, zeolite or mesoporous silica channels, etc. are used as hard templates whereas surfactant micelles, liquid crystals, block copolymer assemblies, etc. are used as soft templates. Self-assembled nanoparticle templates lie in between these two categories because of the "hard" nature of nanoparticles (silica or polymer) and the "soft" spatial arrangement of the template [3]. Template-directed materials have been largely exploited in power sources applications [4, 5] and their use for other purposes (i.e., electroanalysis and sensors) has emerged recently [1, 3, 5, 6].

Direct electrodeposition of metal nanostructures can be formed by electrochemical reduction of the appropriate metal ion through porous membranes (track-etched polycarbonate, anodized alumina [7, 8]), within regularly arranged monodisperse micro-spheres (i.e., polystyrene or silica beads with diameters ranging typically between 100 nm and 2 μm) onto solid substrates [9–11], or in the aqueous domains of lyotropic liquid crystalline phases formed by self-assembly of

amphiphilic molecules [12, 13]. Film porosity is then revealed by template extraction, which can be made by dissolution, solvent extraction, or calcination, thus creating interconnected macro- and/or mesopores in the solid skeleton constructed in the former interstitial spaces defined by the template. The resulting metallic nanostructures are characterized by electroactive surface areas higher by ca. 1–3 orders of magnitude with respect to their geometric surface ones [1, 6, 8, 12, 14, 15].

Indirect electrogeneration of porous and structured layers of metal oxides has also proven to be possible through surfactant template assemblies. A first approach is the cathodic deposition of metal oxide films via alkaline precipitation of metal ions induced by pH modulation at the electrode/solution interface [16–20]. As an example, lamellar ZnO films containing ordered lamellar structures can be obtained when anionic surfactants are added to the plating solution as structure directing agents, as a result of electrochemical interfacial surfactant templating [16–18]. The driving force of the process is the in situ formation of meta-stable amphiphilic assemblies on the working electrode, which are instantaneously captured by the inorganic deposits, resulting in the formation of new phases and new orientations of inorganic mesoporous structures [21]. In our group, we have discovered that oriented mesoporous sol–gel films can be also produced by electrochemically driven cooperative self-assembly of surfactant micelles and silica formation resulting from electrogeneration of hydroxyl ions likely to catalyze the polycondensation of metal alkoxide precursors around spatially arranged amphiphilic molecules at the electrode/solution interface [22]. Thicknesses of these films can be controlled by both the applied potential and duration of the deposition process, typically in the micro- or submicrometric range [23]. A unique feature of these highly ordered silica films is that they exhibit mesopore channels oriented normal to the underlying electrode surface (i.e., an optimal configuration to ensure fast diffusion processes, as required in most electroanalytical methods [1, 3], which remains difficult to prepare to date by conventional evaporation-based sol–gel film formation methods) [24–30]. Such electro-assisted self-assembly (EASA) method can be also applied to prepare functionalized silica layers in one step, by co-condensation of tetraethoxysilane (TEOS) and suitable organoalkoxysilanes [30]. Nevertheless, applying sol–gel co-condensation in electrochemical interfacial surfactant templating is only possible up to a certain level of organo-functional group loading: for hybrid films prepared by EASA, the ordered mesostructure and pore orientation was maintained for molar ratios of organosilane-to-TEOS up to 60 % for methyl groups [31], 10 % for amine [32, 33] and thiol moieties [34], and 8 % for ethylenediamine [35]. Above these values, the transient surfactant hemimicelle assemblies on the electrode surface under potential control is thought to be disturbed and cannot properly induce the growth of an ordered and oriented mesostructure. Another alternative strategy, which was recently proposed as a versatile platform towards hybrid films with perpendicular mesochannels, is the electrochemically assisted generation of highly ordered azide-functionalized mesoporous silica combined to subsequent "Click Chemistry" [36].

The goal of the present study is to extend the above EASA method to the generation of oriented mesoporous thin films bearing long-chain alkyl groups covalently attached to the mesopore channels, which are expected to exhibit distinct hydrophobic-to-hydrophilic balance. These organic groups will be introduced into the film by direct co-condensation of octyltrimethoxysilane (O-TES) or hexadecyltrimethoxysilane (HD-TES) and TEOS, and their content will be varied in order to define the maximal functionalization level that can be reached without loosing the oriented hexagonal mesostructure. The resulting layers will be characterized by various physico-chemical techniques and their permeability properties will be investigated through electrochemical monitoring of redox probes transport rates across the films in order to evaluate the effect of increasing their hydrophobic character upon incorporation of C_8 and C_{16} alkyl chains. Although some previous reports dealing with C_n-functionalized mesoporous silica films obtained by evaporation are available [37–41], the present work constitutes the first example of electrogenerated and oriented mesoporous films of such nature.

Experimental

Chemicals and reagents

TEOS (98 %, Alfa Aesar), O-TES (96 %, Aldrich), HD-TES (96 %, Aldrich), cetyltrimethylammonium bromide (CTAB, 99 %, Acros), ethanol (95–96 %, Merck), sodium nitrate ($NaNO_3$, 99 %, Fluka), and HCl (37 %, Riedel de Haen) were used as received for film synthesis. Film deposition was made onto indium-tin oxide (ITO) plates (surface resistivity 8–12 U, Delta Technologies). Analytical grade ferrocene dimethanol ($Fc(MeOH)_2$, Aldrich), potassium hexacyanoferrate(III) ($K_3Fe(CN)_6$, Fluka), ruthenium hexamine chloride ($Ru(NH_3)_6^{3+}$, Aldrich), and tris(2,2′-bipyridine) ruthenium(II) chloride hexahydrate ($Ru(bpy)_3Cl_2 \cdot 6H_2O$, Acros Organic) were used as redox probes for the electrochemical monitoring of mass transport properties of the films. Potassium hydrogen phthalate (KHP, Fluka) was used as pH buffer. All solutions were prepared with high purity water (18 MΩ cm) from a Millipore milli-Q water purification system.

Electrogeneration of thin films

Organically modified mesoporous silica thin films were prepared by the electrochemically assisted self-assembly (EASA) method described elsewhere [22, 23]. The starting sol solutions consisted of typically 20 mL of ethanol, 20 mL of an aqueous solution of 0.1 mol L^{-1} $NaNO_3$, TEOS, and alkylsilane precursors at various molar ratios ($[Si]_{total}$= 100 mmol L^{-1}), 32 mM CTAB (such 0.32 CTAB/silane molar ratio is the optimal one to obtain regular mesoporous structures by EASA [23]), and a suitable volume of 0.1 mol L^{-1} HCl in order to reach pH 3. Organoalkoxysilanes were introduced in the medium at molar ratios up to 30 mol%. Sol solutions were allowed to hydrolyze for 2 h under stirring at room temperature in order to produce the hydrolyzed precursors.

Afterwards, this solution was introduced in a home-made electrochemical cell in contact with the ITO plate (delimited surface=10 mm inner diameter); a stainless steel counter-electrode and an Ag wire pseudo-reference electrode completing the device. A cathodic potential of −1.3 V was then applied for 30 s in order to generate the necessary hydroxyl ions likely to accelerate the condensation of the (organo)silica precursors. The electrode was quickly removed from the solution and immediately rinsed with pure water to prevent any formation of an unwanted silica layer by evaporation. The deposit was finally dried and aged overnight in an oven at 135 °C. Surfactant extraction was carried out by immersing the film in an ethanol solution containing 0.1 mol L^{-1} HCl for 15 min under moderate stirring.

Characterization of the electrogenerated silica films

All electrochemical measurements were carried out at room temperature with a μAutolab III potentiostat (EcoChemie - Metrohm, Switzerland) monitored by General Purpose Electrochemical System Software. Experiments were carried out in a three-electrode cell using a stainless steel foil as counter-electrode, an AgCl/Ag reference electrode (Metrohm), and the film-functionalized ITO as working electrodes. The film permeability was characterized by cyclic voltammetry (qualitative analysis) and hydrodynamic amperometry (quantitative analysis) using $Fe(CN)_6^{3-}$, $Ru(NH_3)_6^{3+}$, $Ru(bpy)_3^{2+}$, or $Fc(MeOH)_2$ as electroactive probes (0.5 mmol L^{-1} in 0.05 mol L^{-1} potassium hydrogen phthalate, pH 4). Cyclic voltammograms were recorded at a scan rate of 50 mV s^{-1}. Quantitative analysis of permeability through the mesoporous silica films was performed by hydrodynamic amperometry in the flowing mode [42, 43] using a home-built wall-jet electrochemical setup. It consisted in a syringe needle positioned 1 mm from the analyzed film, perpendicular to the film surface (pointing to the center of the electrode surface area defined by a seal (0.4 mm inner diameter)). A platinum wire and an AgCl/Ag reference (Metrohm) complete the device. Volume flow rates (v) were controlled by a peristaltic pump.

The film morphology was characterized by transmission electron microscopy (TEM) using a Philips CM20 microscope at an acceleration voltage of 200 kV. The samples were prepared by mechanically removing some pieces of the films which were then supported on a carbon-coated copper grid. X-ray Photoelectron Spectroscopy (XPS) analyses were performed using a KRATOS Axis Ultra X-ray photoelectron spectrometer (Kratos Analytical, Manchester, UK) equipped with a monochromated AlKα X-ray source (hν=1486.6 eV) operated at 150 W. The base pressure in the analytical chamber was 10^{-9} mbar during XPS measurements. Wide scans were recorded using analyzer pass energy of 160 eV and narrow scans using pass energy of 20 eV (instrumental resolution better than 0.5 eV). Charge correction was carried out using the C(1s) core line, setting adventitious carbon signal (H/C signal) to 284.6 eV. Fourier transform infrared spectroscopy (FTIR) was applied to assess the presence of organic groups in the final materials using a Nicolet 8700 apparatus equipped with a diffuse reflectance accessory (Smart Collector). Contact angle measurements were carried out by the dropping of ultra pure water (V=20 μL) on the surface of silica films using the contact angle meter (Digidrop contact angle meter, GBS Instruments).

Results and discussion

Physicochemical characteristics of alkyl-modified mesoporous silica thin films

Examination of the obtained CTAB-templated alkyl functionalized mesoporous silica films by high resolution TEM (Fig. 1) reveals the existence of an ordered hexagonal mesostructure (top views) with mesopore channels oriented normal to the underlying electrode surface (cross-section views), consistent with other mesoporous silica films prepared by EASA [22, 23, 31–36]. Good level of order and vertical orientation were however maintained only up to 20 % O-TES and 5 % HD-TES in starting sol. At higher functionalization levels, the films became less and organized at the mesoporous level (see, e.g., 30 % O-TES and 10 % HD-TES in Fig. 1). Such limitation was previously reported for other functionalized mesoporous silica films prepared by EASA, and can be explained by the fact that too high contents of organosilane contribute to prevent the self-assembly process (destructuration of surfactant template assemblies) [32, 36]. Note that Guillemin et al. [31] reported the possibility to get highly ordered and methyl-functionalized mesoporous silica films up to 50–60 % of methyltriethoxysilane precursors in the starting sol but the methyl group is much smaller than the long

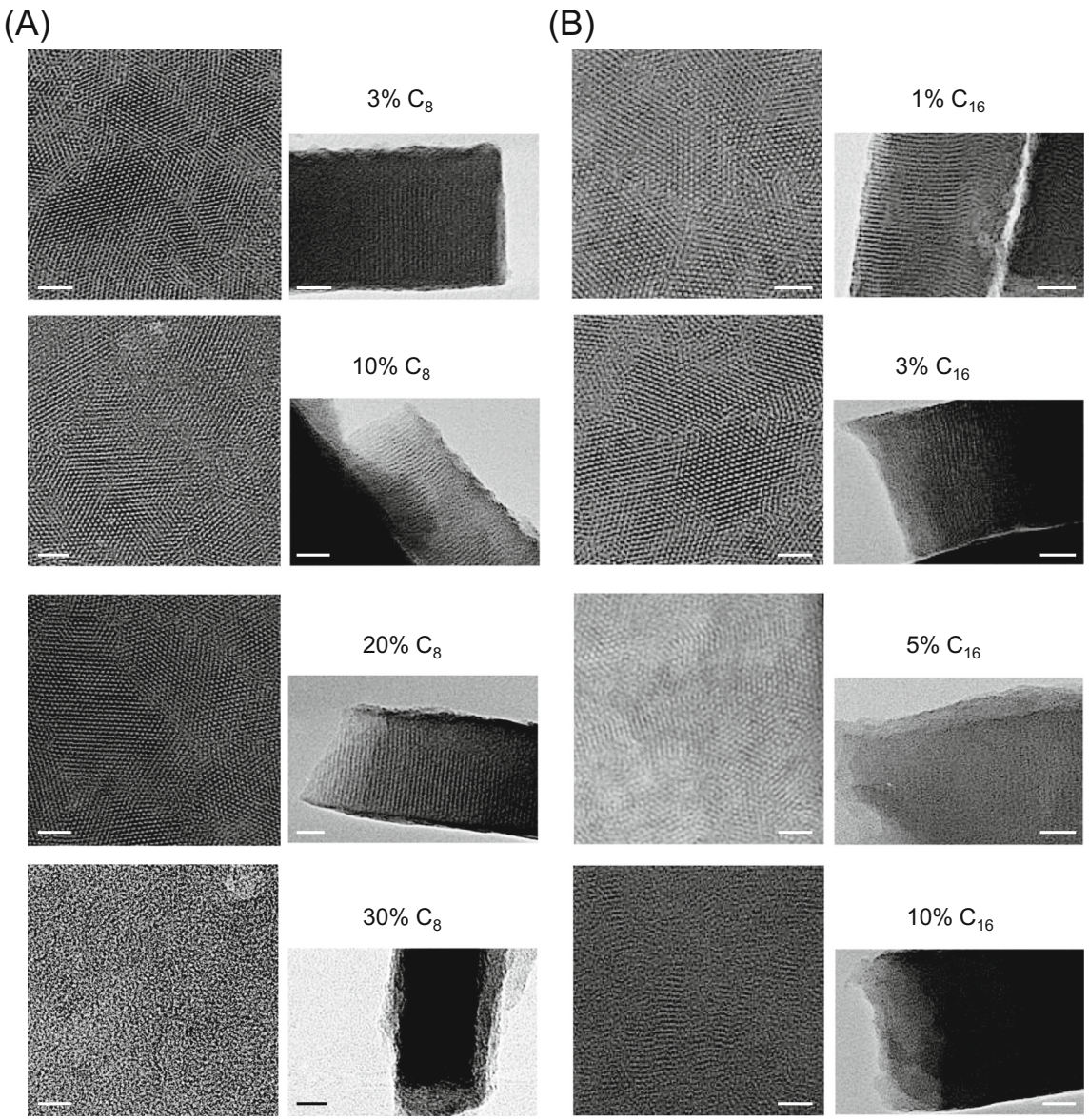

Fig. 1 TEM micrographs of alkylated mesoporous silica thin films incorporating various **a** octyl- and **b** hexadecyl-triethoxysilane contents in the starting sol. *Scale bar*, 25 nm

alkyl chains used here and thus likely to induce less damage to the surfactant assemblies. This is the first example of alkyl-functionalized mesoporous silica films with vertically aligned pore channels closely packed in a hexagonal geometry, thanks to the EASA technique [23] likely to associate an electrochemical interfacial surfactant templating process [44] to an electrochemically driven pH increase necessary to catalyze the polycondensation of metal alkoxide precursors at an electrode/solution interface [45].

XPS and FTIR were then used after template extraction to evidence the presence of alkyl groups in the materials. As show on the narrow binding energy window corresponding to C1s in the XPS spectra (Fig. 2), an additional contribution of the C1s signal located at 282.1 eV appeared for the alkyl-functionalized samples (Fig. 2b, c). This peak, which was not present on the spectra relative to the unfunctionalized mesoporous silica film (Fig. 2a), is attributable to the Si–C bond, confirming the effectiveness of the co-condensation process and successful incorporation of the alkyl groups in the films. As expected from the different amounts of carbon atoms in the alkyl chains (C_8 and C_{16}), the relative contribution of the peak located at 282.1 eV in the C1s signal was lower in case of the longer alkyl chain. Furthermore, FTIR analyses (Fig. 3) give other evidences of the incorporation of the alkyl chain in the silica film. This can be seen on the whole spectra (Fig. 3a, b) via both the absorption band located at 1,230 cm^{-1}, which corresponds to vibration of the Si–CH_2-R moieties and the absorption band of methyl (-CH_3) and methylene (-CH_2-)

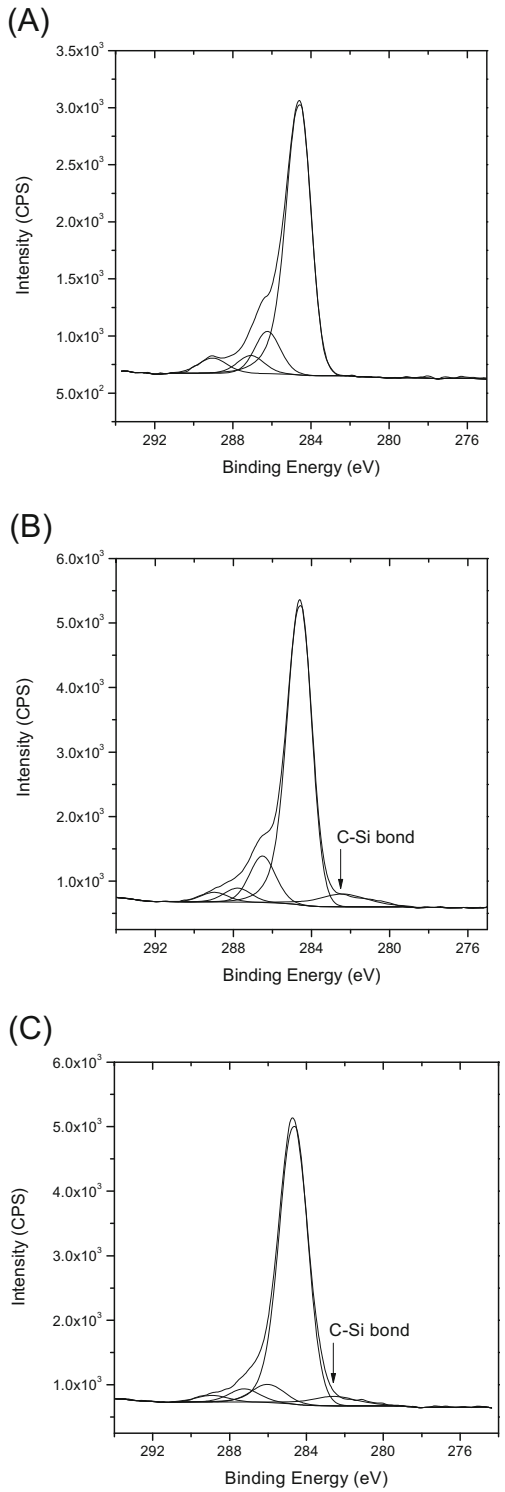

Fig. 2 XPS spectra recorded on **a** non-functionalized; **b** octyl-; and **c** hexadecyl-functionalized mesoporous silica thin films for 3 % of O-TES or HD-TES introduced in the starting sol. Focus on the C1s area (280–290 eV)

groups in the 2,800–3,000 cm^{-1} region [46]. The absence of noticeable bands in the 980–900 cm^{-1} region, i.e., in relation of the cetyltrimethylammonium groups, shows that the extraction of surfactant species was completed. Therefore, the asymmetric -CH_2- stretching vibration at 2,930 cm^{-1} can be attributed unambiguously to the presence of alkyl chains incorporated within the silica films (and not to any residual content of CTA^+).

Accurate quantification of alkyl group contents in the films is not an easy task, especially because elemental analysis is prevented due to too low amount of available matter. Nevertheless, the extent of functionalization can be evaluated from FTIR data, via the variation of the intensity of the vibration band located at 2,930 cm^{-1} (-CH_2- stretching). As shown (Fig. 3c, d), the intensity of this characteristic band increases linearly, respectively, up to 20 % O-TES and 5 % HD-TES in the starting sol, and then tended to level off. These maximal values correspond also to the limits up to which a mesostructure can be maintained (Fig. 1). Such restrictions in the incorporation ratio of O-TES and HD-TES can be explain by the fact that the increase of the alkyl chain length of the alkylalkoxysilane plays a role both on the steric effect and the hydrophobic character towards the accessibility of H_2O molecule during the hydrolysis step [40, 47]. In addition, Shimojima et al. [48] have reported that the structural ordering of mesoporous silica is mainly governed by the degree of polycondensation in the precursor solution and that the alkylsilane condensation rate decreased by increasing length of the alkyl chain, confirming the higher degree of ordering observed here for octyl-functionalized films than for the hexadecyl-ones. XPS analyses also confirm this trend. For example, the C1s signal of octyl-functionalized films was found to increase linearly with the O-TES content in the synthesis sol up to 20 mol% and then tended to level off at higher contents. Additionally, monitoring the C1s/Si2p signal ratios and comparing them to the molar ratio of O-TES in the starting sol relative to the total amount of silane precursors enables one to conclude that the functionalization level is directly proportional to the organosilane content in the synthesis medium up to 20 mol% O-TES, but that the C/Si content ratio in the material is ca. two time lower than in the starting sol (due to condensation of organosilanes slower than TEOS [36]).

A last observation is that the films obtained here are uniform and aggregate-free (consistent with the quite low precursor concentration of 100 mM used for film formation [49]) and that film thicknesses (Table 1) remained more or less constant within the experimental error in the 90–100-nm range for the ordered mesostructures, i.e., up to 20 % O-TES and 5 % HD-TES, and then decreased somewhat for higher functionalization levels, due to slower condensation rates (as usually observed for the growth of less ordered mesoporous silica materials [23]).

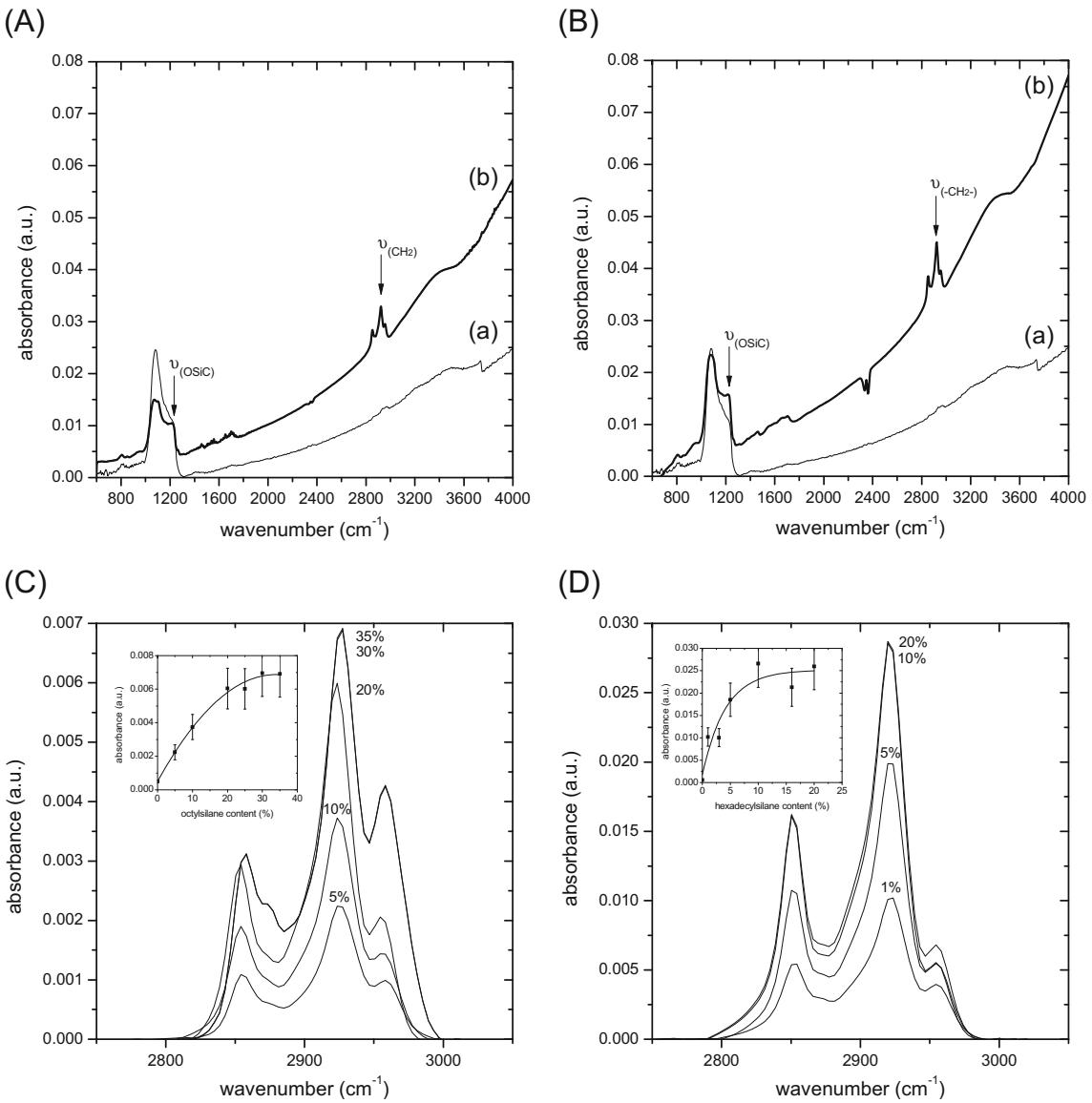

Fig. 3 Diffuse reflectance FTIR spectra recorded in **a**, **b** 600–4,000 cm^{-1} or **c**, **d** 2,750–3,050 cm^{-1} (background substracted) ranges, for alkylated mesoporous silica thin films prepared from sol solutions containing **a**, **b** 3 % of O-TES (**a**) or HD-TES (**b**), or (**c**, **d**) various contents of O-TES (**c**) or HD-TES (**d**). *Inset* (**c**, **d**), variation of the -CH_2- vibration band height (normalized with Si–O vibration band height) versus the quantity of O-TES or HD-TES introduced in starting sol. On parts (**a**, **b**) of the figure, (*b*) represent the curve for alkyl-modified mesoporous silica films, while (*a*) corresponding to unmodified films is given for comparison purpose

Permeability properties of the films

Electrochemical methods are well-suited to characterize mass transport issues through porous silica layers [50]. Qualitative information can be first obtained using cyclic voltammetry (CV). CV recorded before template extraction is likely to check the uniformity of deposition in the form of a crack-free film over the entire electrode surface, which is verified by the absence of any noticeable signal of ionic redox probes in solution (i.e., not likely to reach the electrode surface) and (see Fig. 4a for $Ru(bpy)_3^{2+}$). When using the neutral ferrocene dimethanol ($Fc(MeOH)_2$) probe, only a small response is observed (Fig. 4b), arising from its solubilization into the liquid crystalline phase formed by the surfactant in mesopore channels. In this case, the corresponding CV peaks are shifted to higher potential values than for species in solution due to slower charge transfer processes in this particular environment (stabilization of $Fc(MeOH)_2$ and unfavorable electrostatic interactions between the oxidized $Fc(MeOH)_2^+$ species with CTA^+ cations). After template removal, the film becomes porous to all redox probes. However, in presence of an unmodified silica film, CV curves are affected compared to those recorded on bare ITO as a result of the negatively charged silica surface which induces some accumulation of $Ru(bpy)_3^{2+}$ and larger peak currents (Fig. 4a) while lower signals are observed with $Fe(CN)_6^{3-}$ anions (results not

Table 1 Films thickness evaluated from scanning electron microscopy and characteristic transfer rates determined from wall-jet electrochemistry for mesoporous octyl- and hexadecyl-functionalized silica films

O-TES			
Alkylsilane content[a] (mol%)	Thickness (nm)	$10^{12}\ PD_f$ ($m^2\ s^{-1}$)	
		$Fc(MeOH)_2$	$Ru(NH_3)_6^{3+}$
0	83	8.2	140
5	–	9.6	7.6
10	91	11	3.2
20	74	9.1	0.8
HD-TES			
Alkylsilane content[a] (mol%)	Thickness (nm)	$10^{12}\ PD_f$ ($m^2\ s^{-1}$)	
		$Fc(MeOH)_2$	$Ru(bpy)_3^{2+}$
0	83	8.2	19
5	97	10	34
10	93	5.2	1.8
20	–	0.9	1.6

[a] In the starting sol

shown) due to electrostatic repulsions. The neutral $Fc(MeOH)_2$ probe diffuses almost unhindered through the layer (Fig. 4b). These observations are consistent with those previously reported for related mesoporous silica films [22, 51].

When functionalized with octyl- or hexadecyl- groups, the mesoporous silica thin films (after template extraction) behave quite differently as a function of the organic content in the material, the length of the alkyl group, and the type of redox probe (Fig. 5). If both the charged $Ru(bpy)_3^{2+}$ and neutral $Fc(MeOH)_2$ redox probes are likely to cross the mesoporous films, the intensity of CV responses varies in a significantly different way depending on the functionalization degree and somewhat differently between octyl- and hexadecyl- groups. When using $Ru(bpy)_3^{2+}$, the intensity of CV signals is similar or smaller than on bare ITO (Fig. 5a, c), suggesting some resistance to mass transport and/or less effective accumulation of the positively charged probe by electrostatic interaction with the mesopore surface than for unmodified silica films (Fig. 4a). The decrease in intensity is however much pronounced for hexadecyl- than for octyl-functionalized films, starting respectively at 16 % of O-TES and 3 % of HD-TES (see insets in Fig. 5a, c). This can be roughly explained by the longer chain of hexadecyl- groups, occupying thus more place in the mesochannels and inducing a more hydrophobic character, preventing therefore the ingress of the hydrophilic probe in the material in a more dramatic way. In addition, one has to remind that hexadecyl-functionalized films lose their ordered mesostructure above 5 % HD-TES in the starting sol (Fig. 1b), compared to 20 % O-TES (Fig. 1a), so that this parameter is also though to play an important role in promoting mass transport issues in highly ordered and oriented mesoporous films

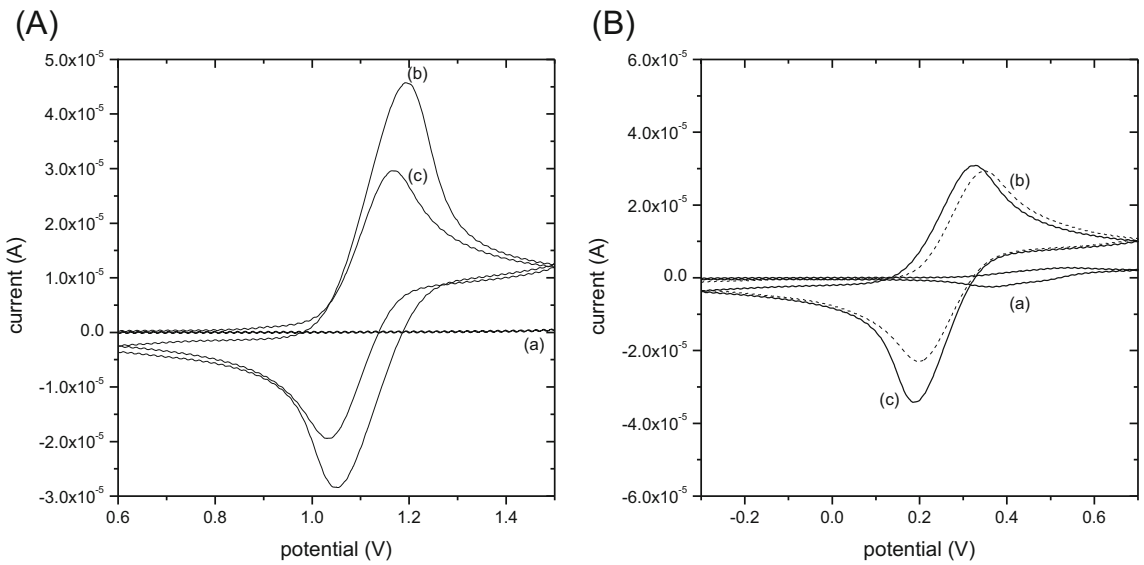

Fig. 4 Typical CV responses of a mesoporous silica thin film to **a** $Ru(bpy)_3^{2+}$ and **b** $Fc(MeOH)_2$ (0.5 mmol L^{-1} in KHP pH 4), respectively, recorded (*a*) before and (*b*) after CTAB surfactant removal; the curve on bare ITO is also shown (*c*) for comparison purposes. Potential scan rate, 50 mV s^{-1}

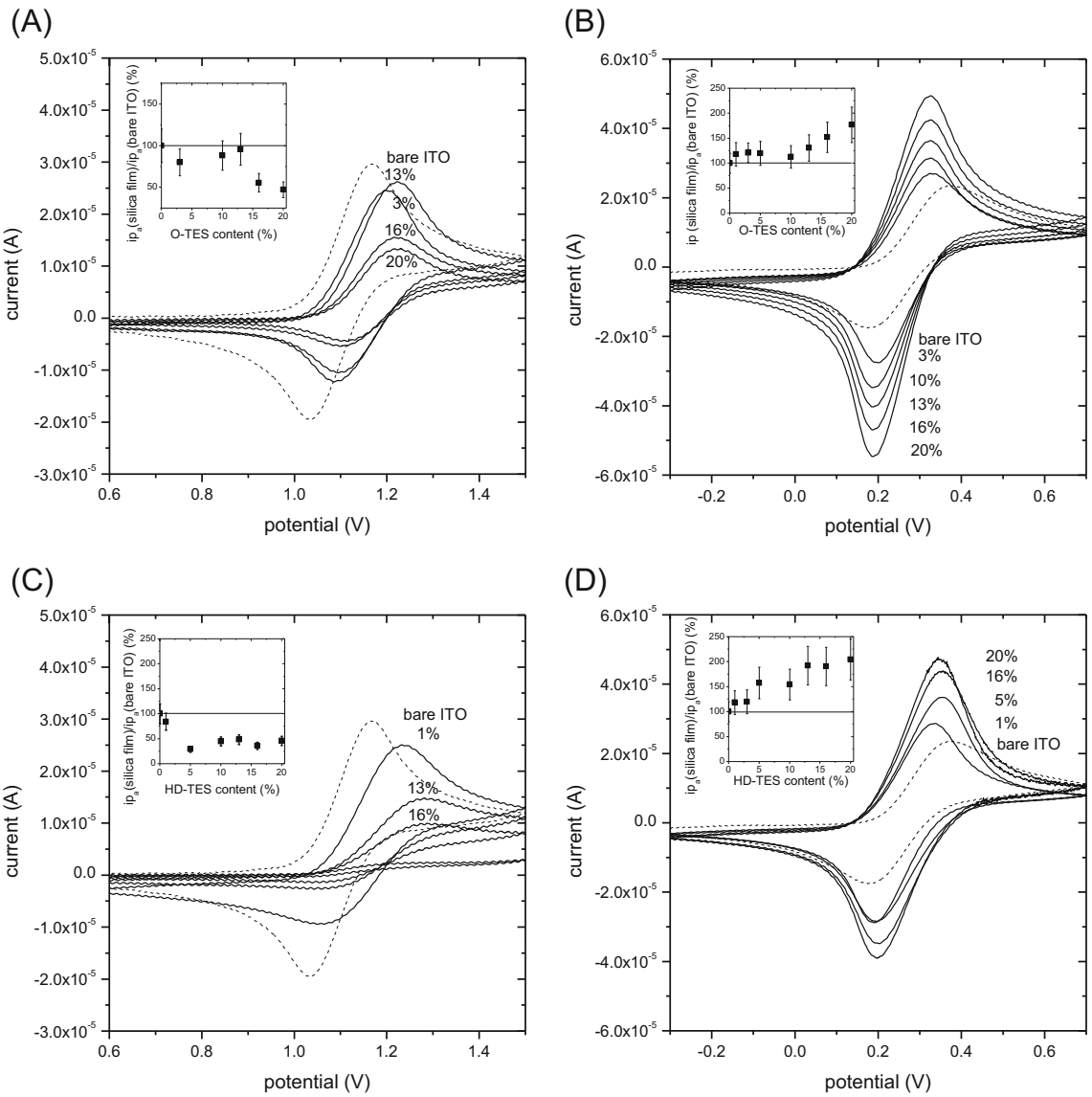

Fig. 5 CV responses of **a**, **b** octyl- and **c**, **d** hexadecyl-functionalized mesoporous silica thin films to **a**, **c** $Ru(bpy)_3^{2+}$ and **b**, **d** $Fc(MeOH)_2$ (0.5 mmol L^{-1} in KHP pH 4), as recorded after CTAB surfactant removal; the films were prepared from starting sols containing increasing contents of organosilane. Potential scan rate, 50 mV s^{-1}. *Insets* represent the variation in peak currents relative to that recorded on bare ITO

(i.e., CV curves close to that on bare ITO for octyl-functionalized films up to 13 % O-TES) and restricting transport rates in less ordered films (i.e., hexadecyl-functionalized films above 5 % HD-TES). Another indication of the effect of hydrophobic groups in the mesopore channels on the electrochemistry of the hydrophilic redox species is the slower charge transfer kinetics observed for the probe in alkyl-functionalized films with respect to bare ITO. Indeed, the oxidation of $Ru(bpy)_3^{2+}$ occurs at more positive potentials and the potential shifts are increasing with the functionalization level and the alkyl chain length ($\Delta E = Ep^{ox}$(modified ITO) $- Ep^{ox}$(bare ITO) = + 40 mV for 3 % O-TES, +60 mV 16 % O-TES, and + 120 mV for 16 % HD-TES).

The behavior of the neutral $Fc(MeOH)_2$ probe is significantly different (Fig. 5b, d). In this case, CV curves are as more intense as higher is the alkyl group content in the film and always larger than signals obtained at bare ITO (see insets in Fig. 5b, d). This indicates an accumulation behavior that is more likely due to the hydrophobic nature of the alkyl chains located in mesopore channels, inducing favorable hydrophobic interactions with $Fc(MeOH)_2$ species. And the effect was even faster for films incorporating longer carbon chain alkyl groups (i.e., C_{16} versus C_8). Such explanation based on hydrophobic interactions is supported by contact angle measurements, indicating an enhanced hydrophobic character of the films bearing octyl- (θ=86°) and hexadecyl- (θ=105°) groups, in comparison to the unmodified mesoporous silica film (θ=

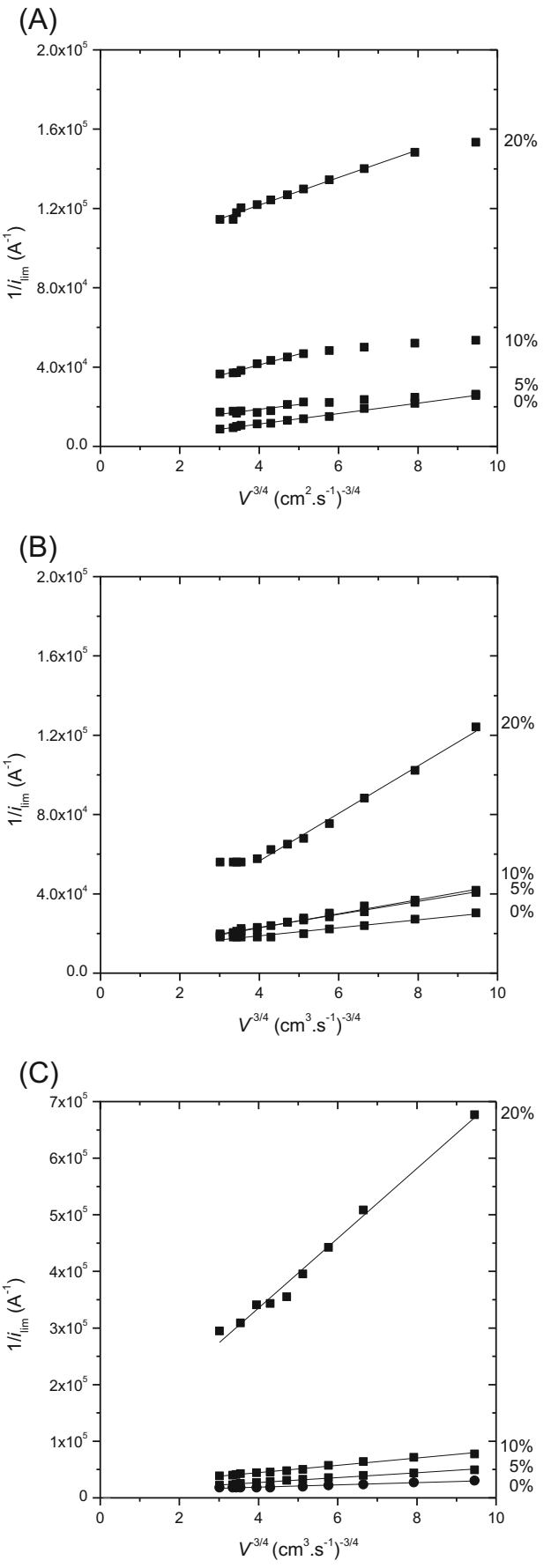

Fig. 6 i/i_{lim} vs $V^{-3/4}$ plots obtained from hydrodynamic amperometry experiments performed in **a** $Ru(NH_3)_6^{3+}$ and **b**, **c** $Fc(MeOH)_2$ (0.5 mmol L^{-1} in KHP pH 4) using ITO electrodes covered by **a**, **b** octyl- or **c** hexadecyl-functionalized mesoporous silica thin films with various alkyl group contents. Applied potentials were +650 $mV_{/Ag/AgCl}$ and −400 $mV_{/Ag/AgCl}$, respectively, for $Fc(MeOH)_2$ and $Ru(NH_3)_6^{3+}$

60°). On the basis of such increases in CV signals, one can conclude that accumulation processes become predominant over restrictions to mass transport expected from mesopore filling with the alkyl groups. Note that no accumulation effect was observed for methyl-functionalized films [31], bringing to the front the importance of the long-chain alkyl groups to impart a sufficiently hydrophobic character to the mesopore channels to enable effective accumulation of hydrophobic solutes. This trend was further confirmed by additional experiments based on short-chain propyl-functionalized mesoporous silica films for which the CV response to $Fc(MeOH)_2$ was decreased by ca. 20 % with respect to bare ITO (for 5 % alkyl- group in the film, data not shown), indicating no noticeable accumulation.

More quantitative information on transfer processes in the films can be obtained from hydrodynamic amperometry. Briefly, Eq. 1 gives the relationship between the diffusion-limited current, i_{lim}, and the current due to mass transport through the solution, i_{MT}, and permeation through the film, i_{perm}. We applied here the method developed and validated by Massari et al. [52] based on wall-jet electrochemistry. It consists of a planar electrode (wall) with known area, A, and a flow of redox probe solution (jet) that provides well-defined hydrodynamics normal to the electrode. A stagnant layer exists in the region closest to the electrode in which mass transport is only controlled by diffusion. Applying a constant volume flow rate, V, of probe solution allows us to measure a steady-state current (i.e., diffusion-limited current, i_{lim}) at the electrode surface subjected to a suitable applied potential (i.e., fitting with the apparent redox probe potential). Increasing this flow rate results in a corresponding increase of i_{lim}. The permeabilities (i.e., product of diffusion coefficient in the film, D_f, and solution-to-film partition coefficient, P) of redox species into the modified silica thin films are deduced from the analytical expression (Eq. 1), which becomes even simpler (Eq. 2) at infinite flow rate (i.e., $1/i_{MT}=0$) [42, 52].

$$\frac{1}{i_{\lim}} = \frac{1}{i_{MT}} + \frac{1}{i_{perm}} = \frac{\upsilon^{5/12}\alpha^{1/2}}{1.38nFCD_s^{2/3}R^{3/4}V^{3/4}} + \frac{d}{nFA(PD_f)C} \quad (1)$$

$$\frac{PD_f}{d} = \frac{i_{\lim}(V\to\infty)}{nFAC} \quad (2)$$

where d is the thickness of the mesoporous film, P is the partition coefficient, C is the concentration of the redox probe in solution, υ is the kinematic viscosity of the solution, R is the radius of the wall electrode, α the diameter of the solution jet, Ds is the diffusion coefficient for the probe in solution, F is the Faraday constant, n is the number of exchanged electrons, and A is the electrode area (defined by a O-ring).

Typical results for long-chain alkyl-functionalized mesoporous silica films, using two distinct redox probes ($Fc(MeOH)_2$ and $Ru(NH_3)_6^{3+}$), are shown on Fig. 6. For all experiments, a linear relationship between $1/i_{lim}$ and $1/V^{3/4}$ is observed (except few small deviations, as also reported elsewhere [43]). For the $Ru(NH_3)_6^{3+}$ probe, the curves were parallel to each other (Fig. 6a), according to Eq. 1, and the extracted PD_f values (Table 1) are continuously decreasing with increasing the functionalization level, as expected from stronger resistance to mass transport through the film due to the presence of higher contents of alkyl groups in the mesopore channels. In such case, no significant accumulation of the hydrophilic probe is expected to occur in the hydrophobic film ($P \approx$ constant), so that the decrease in PD_f values can be mainly related to a decrease in the apparent diffusion coefficient of the probe in the film, in agreement with previous observations [31]. For instance, a silica film prepared in presence of 5 mol% of O-TES in the starting sol exhibits a slower diffusion rate by one order of magnitude compared to an unmodified silica film, and the drop in PD_f values is lower by one more order of magnitude for the 20 mol% O-TES film (Table 1). When using $Fc(MeOH)_2$, the curves are not parallel to each other (Fig. 6b, c), indicating some deviation to Eq. 1, which might be due to the hydrophobic interactions of the probe with the alkyl-functionalized film. Nevertheless, PD_f values can be also estimated from these data and the trend with respect to the functionalization level is significantly different from that observed for the hydrophilic $Ru(NH_3)_6^{3+}$ probe (Table 1). This time, PD_f values first increase slightly with increasing the alkyl group content in the materials and then decrease at larger contents, in a more dramatic way for hexadecyl than for octyl groups. This clearly indicate a dual effect: the increase in alkyl group content contributes to enhance the accumulation properties of the film (as discussed above), leading to larger P values (more effective partition) and thus also larger PD_f values, but increasing further the alkyl group content leads to less and less available place in the mesopore channels for mass transport, resulting in slower diffusion rates (smaller D_f values) and thus contributing this time to reduce the PD_f values. And such decrease due to resistance to mass transport was even more important for less ordered films (e.g., 20 % HD-TES sample), as otherwise reported for poorly ordered mesoporous silica films [43]. The hydrodynamic amperometry method thus provide an interesting way, complementary to CV, for characterizing the permeability properties of such alkyl-functionalized mesoporous silica films, by enabling to evidence both accumulation processes and resistance to mass transport.

Conclusion

In this work, we show that the combination of the sol–gel co-condensation route and the EASA method enables one to generate ordered and oriented octyl- and hexadecyl-functionalized mesoporous silica thin films on ITO electrodes using CTAB as surfactant template. The mesostructural order and vertical alignment of mesopore channels are maintained up to, respectively, 20 % O-TES and 5 % HD-TES introduced in the starting sol, these ranges corresponding also to a linear variation of the alkyl group content in the films. After template removal, such films become permeable to external reagents. The electrochemical investigations of permeability properties using distinct redox probes (i.e., positively-charged or neutral molecules) demonstrate on one hand that neutral molecules can be accumulated via hydrophobic interactions in such organically modified mesoporous films and, on the other hand, that resistance to mass transport through the films increases with the amount of alkyl groups present in the materials. For charged and hydrophilic probes, and/or for poorly- or non-ordered thin films, this mass transport restriction becomes the dominant parameter affecting the electrochemical response. Such ordered and vertically aligned hydrophobic mesoporous silica films are expected to be attractive for applications in preconcentration electroanalysis of hydrophobic analytes or in the field of separation processes requiring a modulation of the hydrophilic/hydrophobic balance of a membrane.

Acknowledgments We thank Pr. Cédric Carteret for his help with IR measurements, Aurélien Renard for XPS analysis (LCPME, UMR 7564 CNRS-Université de Lorraine), and Marie-Cécile De Weerd (CP2S, Institut Jean Lamour–UMR 7198, Université de Lorraine) for providing access to the contact angle apparatus. We are also grateful to Carine Cochet, student in Master of Chemistry (Université de Lorraine), for some preliminary works and the rigorous film preparations during her training period.

References

1. Walcarius A, Kuhn A (2008) Trends Anal Chem 27:593–603
2. Lai M, Riley DJ (2008) J Colloid Interface Sci 323:203–212
3. Walcarius A (2010) Anal Bioanal Chem 396:261–272
4. Cheng F, Tao Z, Liang J, Chen J (2008) Chem Mater 20:667–681
5. Drake C, Deshpandes S, Bera D, Seal S (2007) Int Mater Rev 52: 289–317
6. Walcarius A (2013) Chem Soc Rev 42:4098–4140
7. Martin CR, Mitchell DT (1999) Electroanal Chem 21:1–74
8. Moretto LM, Pepe N, Ugo P (2004) Talanta 62:1055–1060

9. Jiang P, Cizeron J, Bertone JF, Colvin VL (1999) J Am Chem Soc 121:7957–7958
10. Bartlett PN, Baumberg JJ, Birkin PR, Ghanem MA, Netti MC (2002) Chem Mater 14:2199–2208
11. Szamocki R, Reculusa S, Ravaine S, Bartlett PN, Kuhn A, Hempelmann R (2006) Angew Chem Int Ed 45:1317–1321
12. Attard GS, Bartlett PN, Coleman NRB, Elliott JM, Owen JR, Wang JH (1997) Science 278:838–840
13. Choi KS, McFarland EW, Stucky GD (2003) Adv Mater 15: 2018–2021
14. Szamocki R, Velichko A, Holzapfel C, Mucklich F, Ravaine S, Garrigue P, Sojic N, Hempelmann R, Kuhn A (2007) Anal Chem 79:533–539
15. Park S, Boo H, Lee SY, Kim HM, Kim KB, Kim HC, Chung TD (2008) Electrochim Acta 53:6143–6148
16. Choi KS, Lichtenegger H, Stucky GD, McFarland EW (2002) J Am Chem Soc 124:12402–12403
17. Tan Y, Steinmiller EMP, Choi KS (2005) Langmuir 21:9618–9624
18. Steinmiller EMP, Choi KS (2007) Langmuir 23:12710–12715
19. Therese GHA, Kamath PV (2000) Chem Mater 12:1195–1204
20. Boeckler C, Oekermann T, Feldhoff A, Wark M (2006) Langmuir 22: 9427–9430
21. Choi KS, Steinmiller EMP (2008) Electrochim Acta 53:6953–6960
22. Walcarius A, Sibottier E, Etienne M, Ghanbaja J (2007) Nat Mater 6: 602–608
23. Goux A, Etienne M, Aubert E, Lecomte C, Ghanbaja J, Walcarius A (2009) Chem Mater 21:731–741
24. Yamaguchi A, Uejo F, Yoda T, Uchida T, Tanamura Y, Yamashita Y, Teramae N (2004) Nat Mater 3:337–341
25. Freer EM, Krupp LE, Hinsberg WD, Rice PM, Hedrick JL, Cha JN, Miller RD, Kim HC (2005) Nano Lett 5:2014–2018
26. Fukumoto H, Nagano S, Kawatsuki N, Seki T (2006) Chem Mater 18:1226–1234
27. Richman EK, Brezesinski T, Tolbert SH (2008) Nat Mater 7:712–717
28. Nagarajan S, Li M, Pai RA, Bosworth JK, Busch P, Smilgies DM, Ober CK, Russel TP, Watkins JJ (2008) Adv Mater 20:246–251
29. Yamauchi Y, Sugiyama A, Sawada M, Komatsu M, Takai A, Urata C, Hirota N, Sakka Y, Kuroda K (2008) J Ceram Soc Jpn 116: 1244–1248
30. Urbanova V, Walcarius A (2014) Z Anorg Allg Chem 640:537–546
31. Guillemin Y, Etienne M, Aubert E, Walcarius A (2010) J Mater Chem 20:6799–6807
32. Etienne M, Goux A, Sibottier E, Walcarius A (2009) J Nanosci Nanotechnol 9:2398–2406
33. Rafiee M, Karimi B, Asl YA, Vali H (2013) Analyst 138:1740–1744
34. Herzog G, Sibottier E, Etienne M, Walcarius A (2013) Faraday Discuss 164:259–273
35. Rafiee M, Karimi B, Arshi S, Vali H (2014) Dalton Trans 43: 4901–4908
36. Vilà N, Ghanbaja J, Aubert E, Walcarius A (2014) Angew Chem Int Ed 53:2945–2950
37. Anastasova S, Milanova M, Manolov I, Czeppe T, Todorovsky D (2007) Bull Mater Sci 30:511–520
38. Shimojima A, Sugahara Y, Kuroda K (1998) J Am Chem Soc 120: 4528–4529
39. Daoud WA, Xin JH, Tao X (2006) Appl Surf Sci 252:5368–5371
40. Jung SB, Ha TJ, Park HH (2008) J Colloid Interface Sci 320:527–534
41. Matheron M, Bourgeois A, Brunet-Bruneau A, Albouy PA, Biteau J, Gacoin T, Boilot JP (2005) J Mater Chem 15:4741–4745
42. Yamada J, Matsuda H (1973) J Electroanal Chem 44:189–198
43. Etienne M, Quach A, Grosso D, Nicole L, Sanchez C, Walcarius A (2007) Chem Mater 19:844–856
44. Chen M, Burgess I, Lipkowski J (2009) Surf Sci 603:1878–1891
45. Shacham R, Avnir D, Mandler D (1999) Adv Mater 11:384–388
46. Colthup NB, Daly LH, Wiberly SE (1990) Introduction to infrared and raman spectroscopy, 3rd edn. Academic, New York
47. Babonneau F, Maquet J (2000) Polyhedron 19:315–322
48. Shimojima A, Umeda N, Kuroda K (2001) Chem Mater 13: 3610–3616
49. Sibottier E, Sayen S, Gaboriaud F, Walcarius A (2006) Langmuir 22: 8366–8373
50. Etienne M, Guillemin Y, Grosso D, Walcarius A (2013) Anal Bioanal Chem 405:1497–1512
51. Etienne M, Sallard M, Schroder M, Guillemin Y, Mascotto S, Smarsly BM, Walcarius A (2010) Chem Mater 22:3426–3432
52. Massari AM, Gurney RW, Schwartz CP, Nguyen ST, Hupp JT (2004) Langmuir 20:4422–4429